JKAU: Mar. Sci., **Vol. 30** No. 2 pp: 33-57 (1441 A.H. / 2020 A.D.)
DOI :10.4197/Mar.30-2.3

Shoreline Change Analysis Along the Rabigh Coast of Saudi Arabia, Using Multi-Temporal Satellite Imagery

Omar A. Alharbi

Geography Department, College of Social Sciences, Umm Al-Qura University, Makkah, Saudi Arabia

oaoharbi@uqu.edu.sa

Abstract. There is a lack of understanding about the impact of coastal activities on the modifications to the Red Sea shoreline of Saudi Arabia. The present work makes use of multi-temporal satellite data and the Digital Shoreline Analysis System (DSAS) application to investigate changes in the location of the shoreline along the Rabigh coastal area over the period of 1986–2019. For an evaluation of trends in the short and long term, the End Point Rate (EPR) and the Linear Regression Rate (LRR) were employed to determine the rates at which shoreline alterations occurred. According to the LRR technique, the maximum erosion and maximum accretion were –23.22 and 18.8 myr^{-1}, respectively, while according to the EPR technique, the maximum erosion and accretion rates were –47.30 and 40.90 myr^{-1}, respectively. Human activity, including infrastructure expansion, port development, and the creation of industrial zones, underpinned the most significant alterations in the coastline structure. From this perspective, the present work affords an overview of the extent of the possible negative impacts on the coastal regime and the likely implications.

Keywords: Remote sensing, Shoreline change, Coastal erosion, Accretion, DSAS, Anthropogenic activities, Rabigh, Red Sea, Saudi Arabia.

1. Introduction

Coastal zones are very dynamic areas, and there are various environmental factors that can impact variability in shoreline morphology (Komar 1998; Woodroffe 2002; Selvavinayagam 2008; Thomas et al. 2010; Pranzini and Williams 2013). Differences in regimes (for example, wave height and wind direction) can also cause morphological changes (Thomas *et al*. 2010; Thomas et al. 2011a, b and Alharbi et al. 2017). However, it is important to determine whether evident changes are only temporary and whether the shoreline may return to its original position after a calming period (Pethick 1996; Esteves *et al*. 2002).

Nonetheless, it is often the case that human activity around coastal zones, including resource usage and urban development, cause long-term changes. This can lead to heightened hazard vulnerability and environmental damage (Bagli and Soille 2003; Mills et al. 2005; Williams *et al*. 2013). Social and economic stresses, including an increase in population, can also cause increased dependence on coastal areas, making them extremely vulnerable. The main reason for this is the misuse of limited resources or the removal of naturally occurring plant life (Balica *et al*. 2012). It is thus crucial to carry out shoreline change mapping when evaluating coastal hazards.

Aerial photograph analysis, historic maps, and different types of topographic survey are all

typically used by researchers to identify longer-term coastal change rates, with many of these methods being effective (examples include Granja and Carvelho 2000; Zhang *et al.* 2002; Esteves et al. 2002; Dobroniak and Anthony 2002; Newsham *et al*. 2002; Silva and Duck 2006; Esteves et al. 2006; Thomas *et al*. 2010; Natesan et al. 2015). Despite this, satellite remote-sensing techniques and geographic information systems (GIS) have lately started to emerge as preferred choices, as satellite data of high resolution are becoming more widely available (El-Raey *et al.* 1999; Moore 2000; El-Asmar 2002; Liu and Jezek 2004; Dewidar 2011; El-Asmar *et al*. 2015; Basiouny *et al*. 2017). Research has indicated that remote sensing methods can be highly effective for evaluating coastline change when used collaboratively with geomorphological and sedimentary data.

However, a key factor to consider during coastal change mapping is the shoreline indicator. It is difficult to identify a suitable position indicator, both in the field and in photographs (Douglas and Crowell 2000; Zhang *et al*. 2002; Pajak and Leatherman 2002; Leatherman 2003; Parker 2003; Thomas *et al*. 2010; Thomas *et al*. 2011a, b). In most research cases, the high-water level (MHWL). In most research cases, mean high-water level (MHWL) is accepted as the primary shoreline definition. However, MHWL is very difficult to identify, and the vegetation line is thus frequently employed for this purpose, since it can be easily detected in aerial photographs and on historic maps (Zhang *et al*. 2002; Rogers *et al*. 2010; Thomas *et al*. 2011a, b). A wealth of research has been carried out around the world investigating shoreline changes caused by environmental factors.

Many studies have also employed geoinformatics to explore shoreline change and related topics. For example, Tett et al. (2003) carried out a study of the coastal lagoons and fjords in Europe and concluded that monitoring regions of restricted exchange (RRE) is of paramount importance. Further, many other features, including wadis, spits, shallow tidal flats, and sabkhas are relevant to the Red Sea coast. The extreme temperatures and evaporation rates occurring in this region are caused by the fact that not enough water is supplied from the Indian Ocean via the Bab el Mandeb Strait at the south end of the Red Sea, as can be seen in Fig. 1. This fact makes the region perfectly illustrative of an area of limited exchange with distinct coastal features, and it must thus be monitored so that effective coastal zone management policies can be established.

A small number of studies have employed remote sensing data to explore coastline changes in the context of the Red Sea. For example, Dewidar (2011) investigated the patterns of shoreline erosion in the Red Sea zone spanning Marsa Alam to Hamata. In this study, the researchers used multi-temporal satellite imagery from 1972 to 2007. Another example is the work of Sagheer *et al*. (2011), who investigated the patterns of accretion and erosion along the Red Sea shoreline in Yemen. El-Asmar *et al*. (2015) explored shoreline changes in Egypt's east coastal region of Hurghada. Further, to assess geological and geomorphological developments along Ras Al-Shabaan shoreline in the Saudi Arabia Red Sea, Nofal and Abboud (2016) used RS image software to investigate two ETM+ images from 1990 and 2010. Coastline changes along the coast of the South-Eastern Red Sea in Saudi Arabia were also studied by Alharbi *et al.* (2017) from the period of 1973–2011 with a Landsat MSS, TM and ETM+ being employed for this purpose. Recently, Niang (2020) observed the shoreline changes along the Yanbu, on the western part of Saudi Arabia, using multi-temporal satellite images from 1965 to 2019. This research primarily aimed to define and measure areas for erosion and

accretion that coastal managers could use to develop and implement effective coastal zone management policies in the area.

2. Physical Setting of the Study Area

As depicted in Fig. 1, Africa and the Arabian Peninsula are divided by the lengthy portion of the Red Sea, stretching along the Sinai Peninsula in the north-west to the Bab el Mandeb Strait in the south-east, which is the point of convergence with the Gulf of Aden. This area is around 1,900 km long, and most of its opposing coastlines are extremely parallel. The Red Sea is only 175 km-wide in the North. However, its width increases further south, reaching a maximum of 350 km near Jizan. However, from here the width once again decreases to as low as 30 km at Bab Al Mandab. Further inland, there is a narrow coastal plain that is only 1–40 km in width. Additionally, the region encompasses an escarpment at an altitude between 1,500 and 3,000 m, which is a major structural component of the Red Sea rift area, and consists of the African and Arabian shield uplifts (Al Sayari and Zotl 1978).

The evolution of the coastline structure is determined by the sub-environments, including sabkhas, intertidal flats, lagoons, sand dunes and wadis (Short and Masselink 1999). In such sub-environments, various factors (including geology, texture and volume of sediment, wind action, waves, and climate differences) come together to create intricate patterns of behaviour (O'Connor *et al*. 2007). To further complicate the situation, other factors, such as the geographic location of offshore islands, nearshore bathymetry, and the shelter that their lees give to beaches, also play important roles (Benedet *et al.* 2004). Moreover, as Carter (1988) points out, morphological variability occurs at temporal scales and can last all the way from a few seconds to a few years.

There is very little rain in this hot, arid area (averaging 6 $cmyr^{-1}$), and there can be as much evaporation as 205 $cmyr^{-1}$ (Behairy et al. 1991). It is primarily during the winter that precipitation occurs. However, there is often no rain for years at a time. In the northern part of the Red Sea, systems of low pressure occasionally develop in the spring, accompanied by atmospheric dust and reduced visibility (Morcos 1970). There can be differences of as much as 10°C (22°C–32°C) in the surface water temperatures according to the season. Variations in humidity also range from 50% in winter to 68% in summer, with humidity being much higher during the day. Patzert (1974) points out that seasonal and regional differences are largely impacted by wind speed and direction, both of which typically increase further northwards. For most of the year, the wind blows from a north-northwest direction and can reach speeds of 7–12 km h^{-1}, while, during winter, a few winds can blow from the south (Durgaprasada Rao and Behairy 1986).

The ancient Saudi city of Rabigh in Makkah Province is situated on the Red Sea's east coast, at latitudes 22° N and 23° N. The city is approximately 130 km north of Jeddah City (Fig. 1a, b). The study area spanned 60 km along the coast, with important features including lagoons and coral terraces. In northern Rabigh City, Al-Kharrar Lagoon can be found, while Sharm Rabigh is situated in the southern area of the Al-Kharrar Lagoon (Fig. 1c). King Abdullah Port, which began service in February 2019, can be found in the centre of the Rabigh coast. The 2005-founded King Abdullah Economic City (KAEC) is the commercial hub of Saudi Arabia and is situated at the southernmost point of Rabigh city (Fig. 1c).

The majority of the shoreline along the Rabigh coast has terrigenous raised coral reefs with marine materials attached through the build-up of old shoreline deposits. Madah *et al.* (2015) points out that the Red Sea is both microtidal and semidiurnal, with the tide

varying slightly from north to south. The biggest tidal ranges occur around the extremities, with the Suez Gulf's entrance and the Aqaba Gulf surrounded by a spring range of 0.6 m. Meanwhile, at the other end, surrounding the Bab el Mandeb Strait, the spring range reaches 0.9 m. Compared to summer, the sea level rises to 0.5 m during winter. Despite a low tidal range between 20 and 30 cm, the water can surge over neighbouring sabkhas during high tide. During this period, the flow of the lagoon water into adjacent sabkhas depends heavily on the prevailing north and north-easterly winds, particularly during storms. Despite this, the sabkhas are impacted by the low tidal range, not through flooding, but by forming a thin water layer (Behairy *et al*., 1991). The Rabigh coast area is separated into a number of siliciclastic-carbonate sediments deposited through an intricate network of climatic and oceanographic processes (Basaham, 2008). Moreover, it is possible that the calcareous sediments present were deposited during the erosion of coastal reef limestone terraces (Al-Washmi, 1999). It is possible for flood sediments to become over 20 m thick (Al-Baroudi, 1990).

In terms of topographic configuration, the key features of this area include low-altitude flat coastal plains from the Hijaz mountains and volcanic lava tongues and harrats, which are created through lineaments and ancient wadis. This lava flows through the paleo-valleys, moving in the direction of the water. This means that a majority of wadis take water from the mountains and then push it to the Red Sea via the coastal plains (Fig. 2). The volcanic tongues and quaternary sediments are significant factors in determining the settlements of the population and the relevant human activities, as people attempt to locate themselves near to available springs and fertile land. Human activities heavily impact the coastal wadi deltas in this area. According to the satellite images observed for the present research, the city extremities include a number of wadis that revert back to their previous course when heavy rains are experienced, regardless of the local urbanization (Fig. 2).

3. Materials and Methods

3.1. Data Used

The study provides information about the Rabigh coast for the periods of 1986, 1998, 2005, and 2019, which shows the satellite image data from multiple sources, such as time points and high spatial resolution. As indicated in Fig. 3, optical satellite images ensured coverage for every period, namely, SPOT-CIB (1986), Landsat TM (1998), Landsat ETM+ (2005), and Sentinel-2 (2019). The optical images include the whole area that is under investigation. The United States Geological Survey (USGS) website (https://earthexplorer.usgs.gov) allows the downloading of the images. A spatial resolution in the range 10–30 m applies to all data. Furthermore, apart from the model from 1986, which was panchromatic, all the pictures were of multispectral type. Table 1 provides information pertaining to each image.

3.2. Image Processing

To perform geometric correction, control points were applied to the reference image, namely, Landsat ETM+ (2005), which served as the basis for correction of the other images; and the images requiring correction determined the number of points. The geometric correction was performed based on the polynomial method using the ERDAS IMAGINE software. Subsequently, the image was projected in the Universal Transverse Mercator (UTM) format in relation to the world geodetic system (WGS)-84 datum (Natesan *et al.,* 2015; Niang, 2020). Once the correction was finalised, it was discovered that the images had a high geometric match, as the root mean square error (RMSE) was not higher than 1 pixel (Maune, 2007). The RMSE represents the space between the ground

control points (GCPs) and the position of the point according to the estimate provided by the adjusted polynomial, and their real positions. After the geometric correction, a number of spectral indices were applied to the images to improve the contrast so as to better identify the reference line. All rectified images were then displayed to the ArcGIS software to digitise the coastline.

3.3 Identification and Markers of the Shoreline

Shoreline characterisation was based on the high-water line (HWL). This common area between land and water was visible on the images due to the contrast between the darker wet beach and the lighter dry beach. Permitting visual interpretation, the HWL is widely thought of as the ideal marker of shoreline location in historical studies of shoreline kinematics, particularly in regions without tide (Crowell *et al*., 1991; Pajak and Leatherman, 2002; Wernette *et al*., 2017). Furthermore, the HWL can be identified without difficulty in the field as well as via image analysis, with a fluctuating margin of error (Pajak and Leatherman, 2002). The region under investigation has been extensively modelled by human hands, and the reference line was therefore equivalent to the harbour area limit in the middle section, which included the section jetties exceeding 20 m (Zhang *et al.*, 2014).

A manual technique was chosen to determine the shoreline in the Rabigh coastal area through visual inspection of digital satellite images. Evaluation based on the contrast apparent in the images enabled definition of the reference line. Nevertheless, the reference line did not go beyond the harbour and/or beach infrastructure expansion for a substantial portion of the coastline. The reference line was mapped or digitised by hand as a vector layer in a linear format with the ArcGIS 10.7 software. In this way, a coastline was produced for each image. This technique is uncomplicated, but its precision depends on the image resolution and the assessment generated by the individual interpreting the photos.

The Superposition of various digitisations of the reference line for several years enabled measurement of the coastline's dynamics. A few of the dimension lines obtained for numerous years are illustrated in Fig. 4.

3.4 Approximation of Uncertainty Concerning Shoreline Location

The precision of the reference line location and implicit dependability of the measurements on how the coastline evolved historically, can be impacted by numerous uncertain sources. These can be classified into two categories: errors introduced by data sources and errors related to methods of measuring and interpreting the coastline (Moore, 2000; Wernette *et al*., 2017). Consideration must also be given to errors in the position of the dimension line in the historical image, errors in georeferencing, errors in the interpretation of the choice and digitisation of the reference line, and errors inherent to the geometry and the resolution of the images. Researchers frequently distinguish numerous forms of unpredictability (Hapke *et al*., 2011; Chentamil Selvan *et al*., 2014), but the present work limited itself to the determination of georeferencing (E_g), coastline digitisation (E_d), and pixel error (E_p) uncertainties. This formula applied to determine the uncertainties (U) related to the yearly shoreline localisation is shown below:

$$(U = \sqrt{E_g^2 + E_d^2 + E_p^2})$$

The quality of the employed diachronic data determined the calculation of the various sources of uncertainty. Despite fluctuating between sources, the georeferencing uncertainty denoting the highest admissible

RMSE is usually low (image orthorectification). The georeferencing error in this study was 2 m in all the periods (Table 2). As listed in Table 2, the pixel error was in the range 10–30 m and impacted the reference line identification while the indicated digitisation error was in the range 5–15m.

A calculation of uncertainty was also performed for the rate of the shoreline modifications. As defined by Hapke et al. (2011), dividing the square root of overall yearly coastline position uncertainties by the number of years between two dates of shoreline survey gives the uncertainty associated with the rate of endpoint (U_r) changes for each transect. This formula can be expressed as:

$$(U_r = \sqrt{\frac{U_1^2+U_2^2}{year2-year1}})$$

In the above, the overall shoreline uncertainties for the first period (year 1) are denoted by U1, while the overall shoreline uncertainties for the final period (year 2) are denoted by U2.

Table 3 shows the estimated error for shoreline change rates for three specified periods. The error was between 1.41 and 5.37 myr^{-1} and represented the average of the shoreline location errors and those correlated with the estimation of the rate of change.

3.5 Measurement and Interpretation of the Rate of Shoreline Modification

The End Point Rate (EPR) and Linear Regression Rate (LRR) for short- and long-term analysis were the approaches used to measure the baseline change rate. The former was used with the sequential shorelines for the periods 1986–1998, 1998–2005, and 2005–2019, while the latter was employed to determine modifications of the shoreline over the entire period from 1986–2019, amounting to 33 years.

For each transect, the short- and long-term change rates were determined via USGS' Digital Shoreline Analysis System (DSAS) version 4.4 (Thieler *et al*., 2017). The DSAS was employed because it is accessible free of charge and is compatible with the ESRI ArcGIS software. In the present work, the DSAS facilitated the creation of orthogonal transects at 100-m distances from one another along the coast as well as the calculation of the statistics related to the modifications based on the EPR and LRR along with four other methods. The total approach adopted to achieve the study goals is detailed by the flowchart shown in Fig. 5.

Determination of shoreline movement and the rate of modification often relies on the LRR statistical method (Crowell and Leatherman, 1999). However, this method fails to consider changes among interim periods that may slow down or speed up modifications (Himmelstoss *et al*., 2018) depending on different factors. This is where the EPR is useful, as it serves to delineate all trends for each transect among various intervals. The measured rate denotes the discrepancy in shore location between two years divided by the amount of time that has passed. Over the duration investigated in the present work, the earliest and latest shorelines were separated by a period of 7–14 years. On this basis, it was possible to recreate the key phases of Rabigh coastline occupation.

The next step was to analyse the coastline kinematics. The analysis was performed at intervals of 100 m along an approximately 60-km north–south stretch of coast in the area under investigation.

3.6 Field survey

Industrial areas along the middle and southern parts of the Rabigh coast were inaccessible. Therefore, GPS was used to undertake a field survey for ground assessment of the uncertain regions. Figure 6 illustrates

several images captured in the context of the field survey.

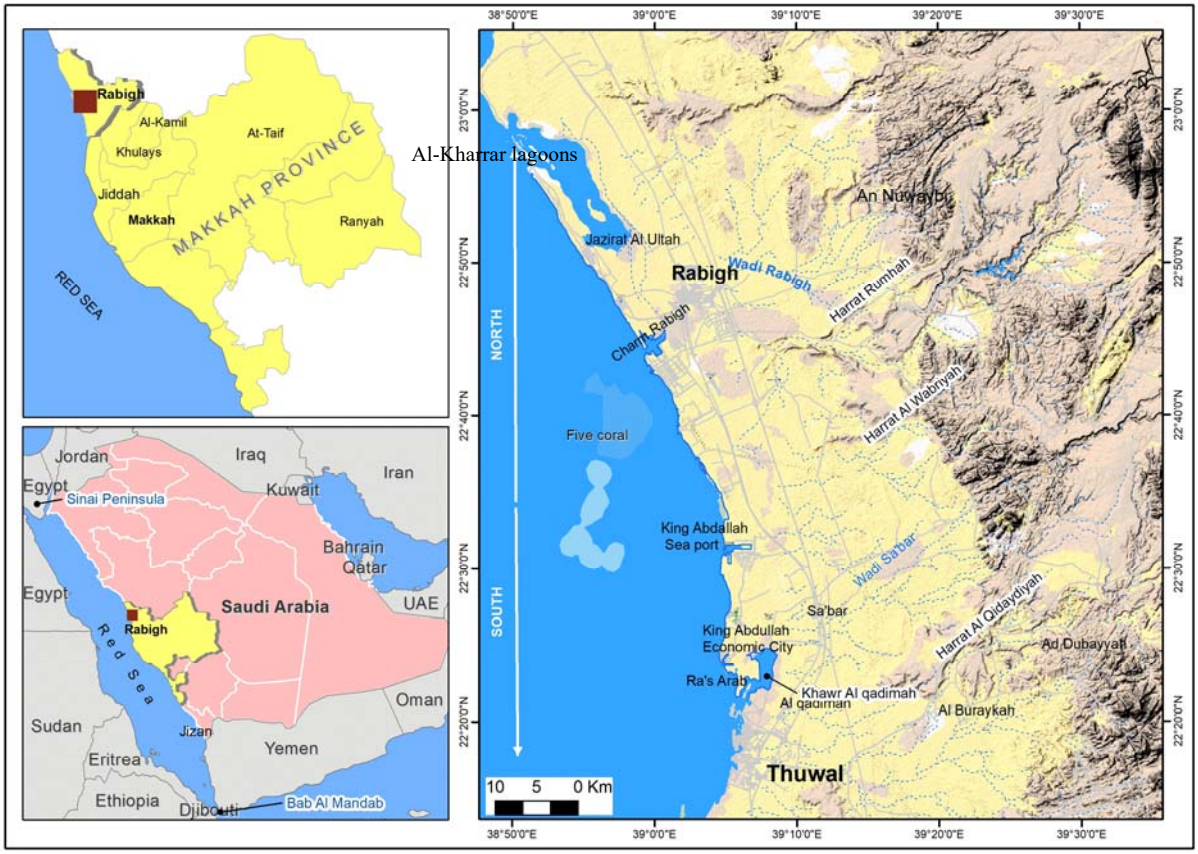

Fig. 1. (a) Kingdom of Saudi Arabia and surrounding coastal regions. (b) Map detailing Makkah province and Rabigh city in the North. (c) Rabigh, the location of the study area.

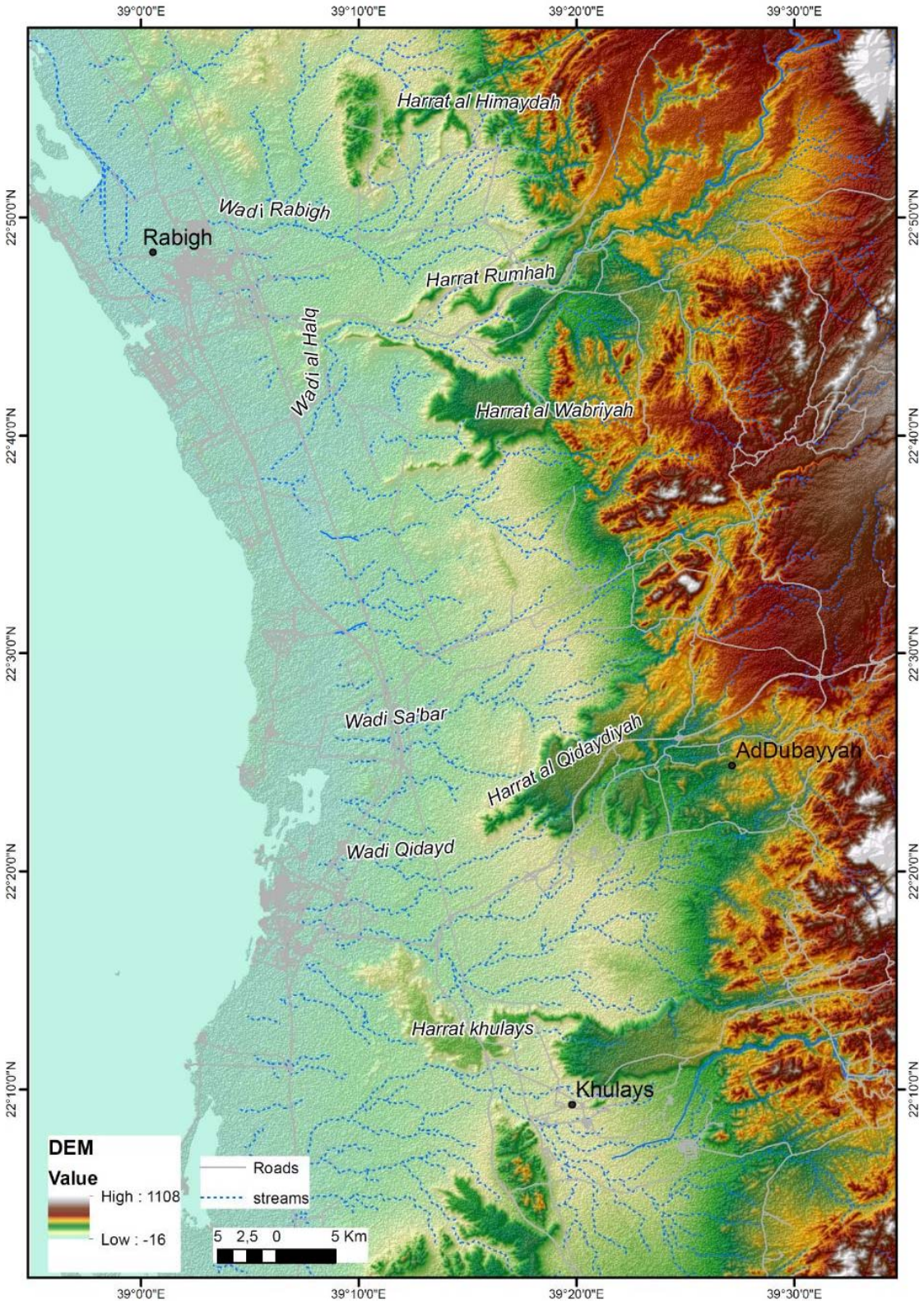

Fig. 2. DEM SRTM showing the topographic context of the study area.

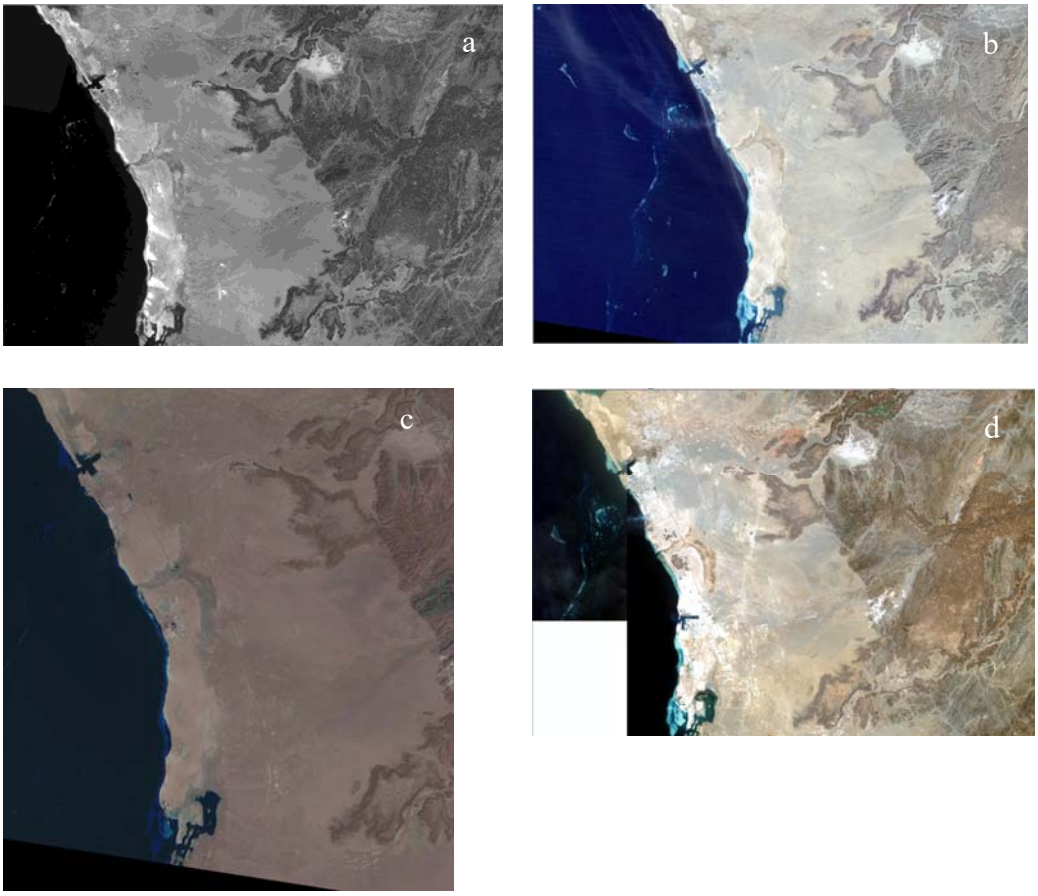

Fig. 3. The employed satellite image data captured at different time points. (a) SPOT-CIB 10 (1986); (b) Landsat TM (1998); (c) Landsat ETM+ (2005); (d) Sentinel-2 (2019).

Table 1. Multi-temporal satellite data used in the study.

Satellite data	Acquisition Date	Band used	Spatial resolution (m)
SPOT CIB 10	03/24/1986	Panchromatic	10 m
Landsat TM	03/20/1998	visible and near-infrared (VNIR)	30 m
Landsat ETM +	01/07/2005	visible and near-infrared (VNIR)	15 m
Sentinel 2	06/06/2019	visible and near-infrared (VNIR)	10 m

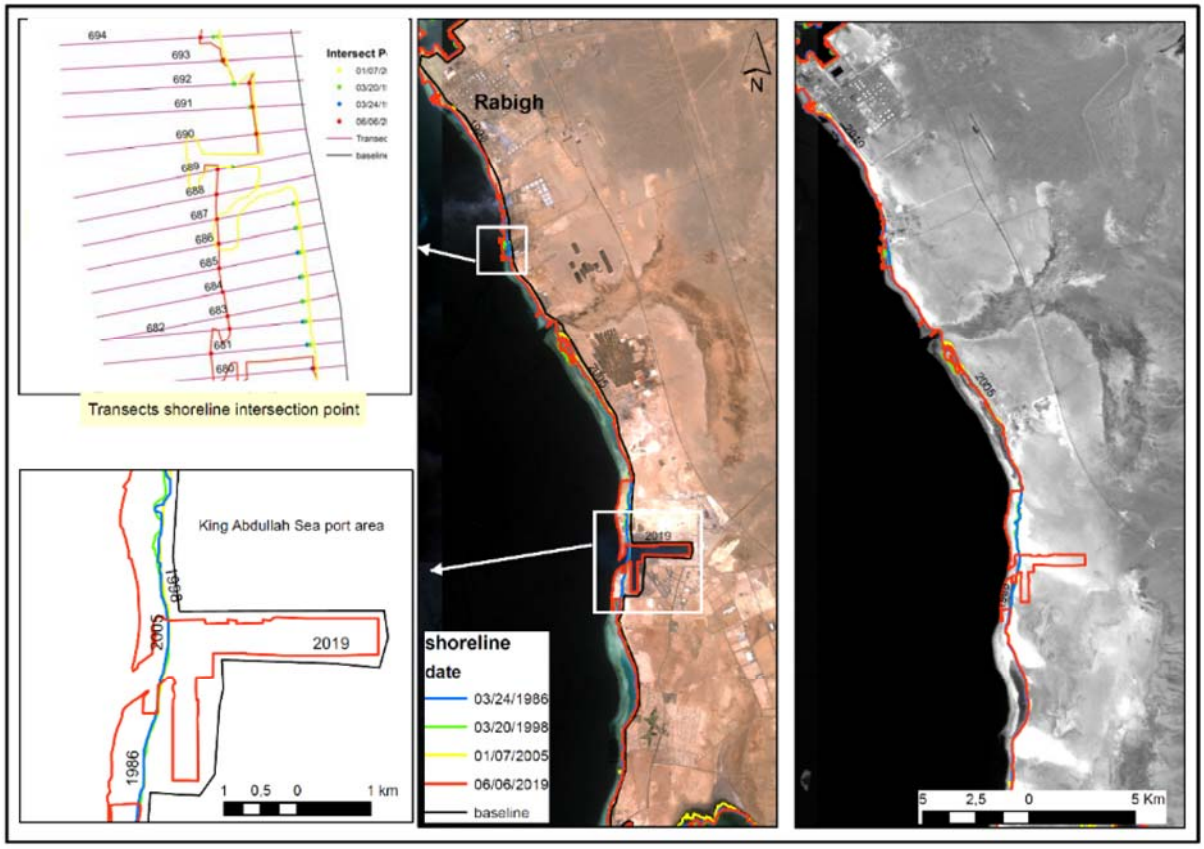

Fig. 4. The shoreline locations derived for multiple time points (Rabigh Power Plant and King Abdullah Port) and the points at which the transect and shoreline intersected, which were employed to determine the change rate.

Table 2. Approximated precision of shorelines extracted from different sources and related average uncertainty.

Types of uncertainty	1986	1998	2005	2019
E_g	2m	2m	2m	2m
E_d	5m	15m	7. 5m	5m
E_p	10m	30m	15m	10m
Total uncertainty (U)	**11.35 m**	**33.6 m**	**16.88m**	**11.35m**

Eg: Georeferencing error, Ed: Digitizing error and Ep: Pixel error

Table 3. Approximated error related to the rate of modifications of the shorelines.

Period	Yearly error (myr^{-1})
1986–1998	2.96
1998–2005	5.37
2005–2019	1.41
1986–2019	1.48

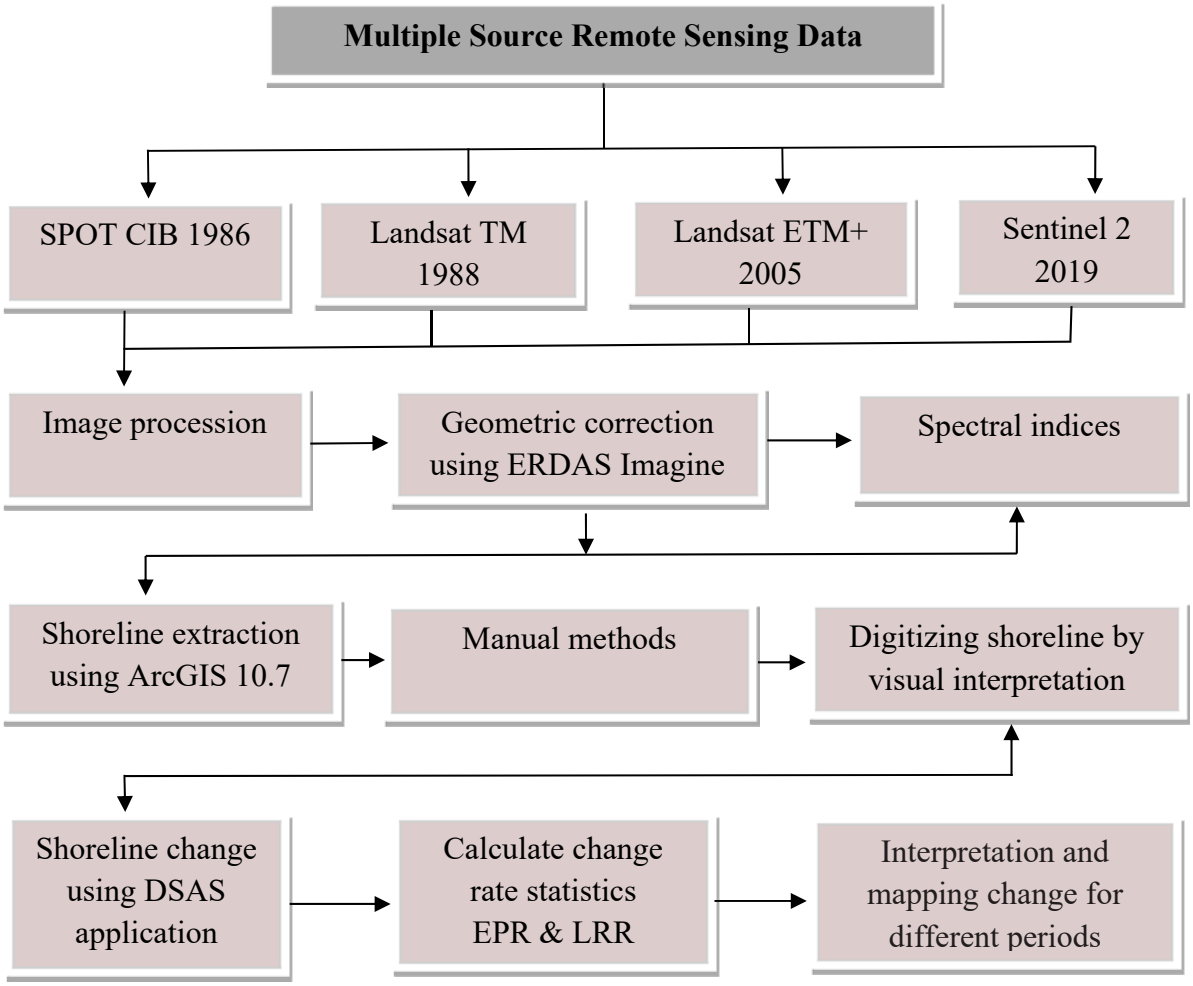

Fig. 5. Flowchart of the approach used in this research.

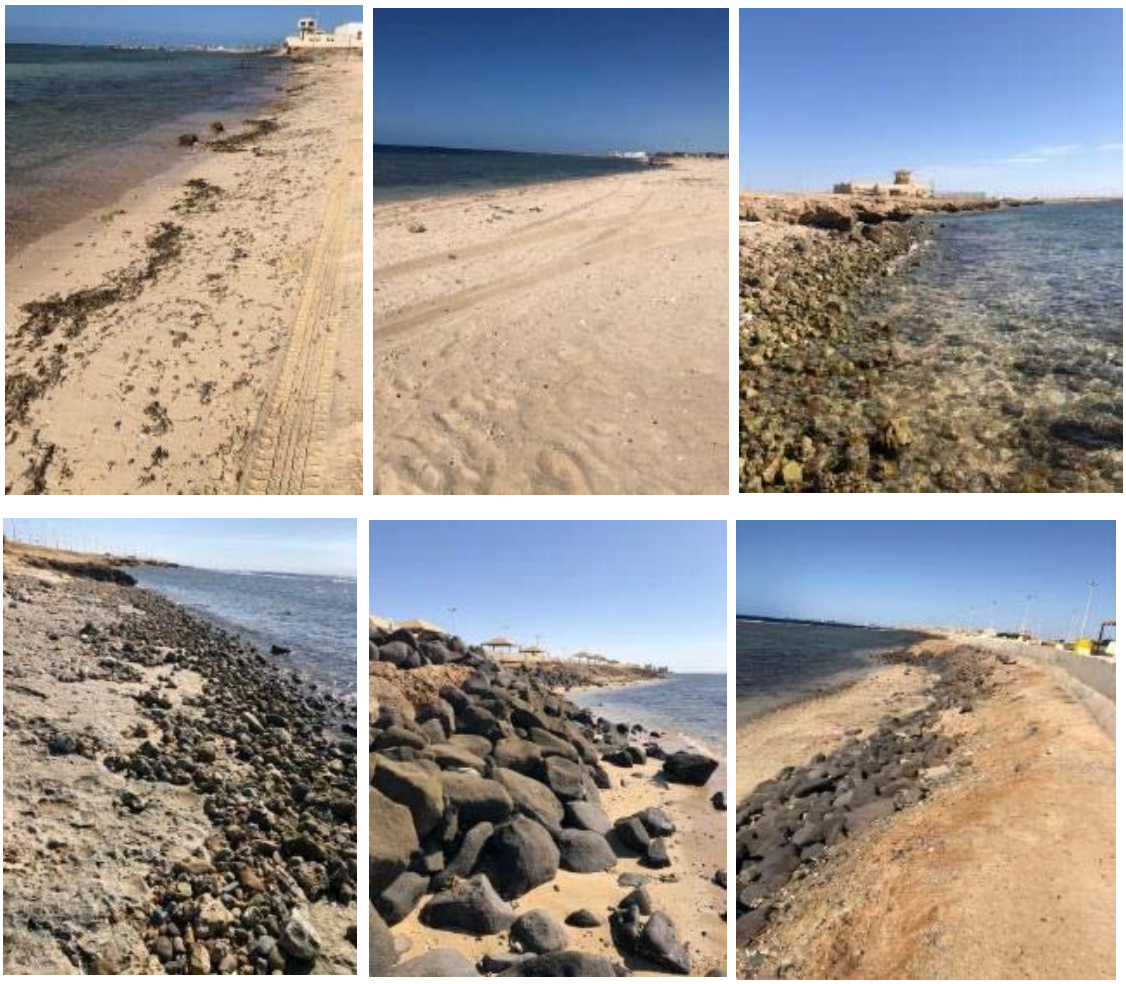

Fig. 6. Field photographs taken along the northern coast of the study area.

4. Results

4.1. Long-term Shoreline Change Rates of the Rabigh Coastline (1986–2019)

The LRR technique was employed to determine how the shoreline changed over the long term in the period of 1986–2019. The rate of modification was computed using this technique by fitting the least square regression to every shoreline at every transect. The general rate of modification of the shoreline that was determined in this manner is illustrated in Fig. 7a and b. According to the overall average rate determined by the LRR, there was a shoreline erosion trend during the research period. More specifically, 82.61% of transects were found to have suffered erosion. However, erosion of statistical significance was exhibited only by 0.11% of transects. Conversely, accretion was displayed by 17.39% of transects, but this was not of statistical significance in any transect. A maximum erosion value of –23.22 ± 0.48 myr^{-1} was recorded in KAEC, south of the study area (Table 4; Fig. 7a and c), and the average erosional rate was –1.14 ± 0.48 myr^{-1}. A maximum accretion value of 18.8 ± 0.48 myr^{-1} was recorded in the Wadi al Halaq (Fig. 2), with the average rate being 4.79 ± 0.48 myr^{-1} (Table 4; Fig. 7 a and c).

Table 4. Estimated LRR and EPR rates for three periods based on DSAS analysis of the shoreline.

Period	Accretion (myr^{-1})		Erosion (myr^{-1})		Average (myr^{-1})
	Max.	Average	Max.	Average	
LRR (1986–2019)	18.8	4.79	–23.22	–1.14	–0.5
EPR (1986 and 2019)	18.78	3.3	–22.13	–1.46	–0.3

Table 4 and Fig. 6b and c show the EPR results. According to the overall average rate for the 1986–2019 period, an erosion trend was displayed by the Rabigh coastline, with erosion affecting 78.73% of the transects, of which 58% had erosion of statistical significance. Meanwhile, accretion was displayed by 21.27% of transects, of which 16.22% had accretion of statistical significance. The maximum erosion value was –22.13 ± 0.48 myr^{-1}, and the average erosional rate was –1.46 ± 0.48 myr^{-1}, while the maximum accretion value was 18.78 ± 0.48 myr^{-1}, with the average rate being 3.3 ± 0.48 myr^{-1}. Accordingly, the EPR (1986 and 2019) indicated the same trends as the LRR (1986–2019; Fig. 7c).

Over the studied period, substantial accretion and/or erosion occurred in a number of areas of the coastline located close to human-made structures. Thus, it was concluded that human activities were a major contributor to these significant alterations in the shoreline (King Abdullah Port had not yet been constructed in 1986). Urban expansion and the introduction of various kinds of infrastructure thus shaped the coastline.

4.2. Short-term Shoreline Change Rates of the Rabigh Coastline (1986–2019)

The short-term trends revealed by the examination of shoreline modifications could be associated with the intensification of shoreline kinematics as well as with transient deceleration or reversal. Such an examination also permits tracking of the evolution of infrastructure emergence along the coast, as is the situation with the coastline in the investigated region, which has been the site of extensive human activity. Hence, the data in the attribute tables produced by the DSAS need to be analysed and interpreted to evaluate how fast the coastline evolved along with its cartography. The coastline development over time was gleaned from the indices suggested by the DSAS, especially the EPR, which facilitated assessment of the evolution between two sequential coastlines. Table 5 and Fig. 8a–d illustrate the EPR outcomes for various year pairs. As can be seen in Fig. 8, over the period of 2005–2019, the highest level of erosion determined by the EPR variation was –47.30 myr^{-1}, with the average being –1.96 myr^{1}. At the same time, the highest level of accretion was 40.90 myr^{-1}, with the average being 4.74 myr^{-1}. The same figure reveals discrepancies between the trends related to the rates of modification in every period.

Table 5. Estimated EPR rates for three periods based on DSAS analysis of the shoreline.

Period	Accretion (myr^{-1})		Erosion (myr^{-1})	
	Max.	Average	Max.	Average
1986–1998	14.68	1.43	–9.76	–6.08
1998–2005	39.35	2.67	–45.89	–3.83
2005–2019	40.90	4.74	–47.30	–1.96

4.2.1. Shoreline Changes 1986–1998

The EPR results for this period, illustrated in Fig. 9a, show that the Rabigh coastline was subject to erosion, with 59.77% of all transects being erosional but only 7.68% of them displaying statistically significant erosion (this is probably linked to the high value of uncertainty at ± 2.96 myr^{-1}). Accretion was exhibited by 40.23% of the totality of transects, of which 5.65% had growth of statistical significance. The maximum erosion value was –19.76 ± 2.96 myr^{-1} (Table 5; Fig. 9a) and was recorded in the middle study area, specifically at the industrial area (Fig. 10), with the average erosional rate being –6.08 ± 2.96 myr^{-1}. The maximum accretion value was 14.68 ± 2.96

myr^{-1} (Table 5; Fig. 9a), with the average rate being 1.43 ± 2.96 myr^{-1}. This value was recorded in the northern part of the industrial area and Sharm Rabigh (Fig. 10). The area displaying the second most accretion (approximately 11 ± 2.96 myr^{-1}) was located in the far south at Khawr al Qadimah due to Wadi Sa'bar flow (Fig. 10).

4.2.2. Shoreline Changes 1998–2005

As depicted in Fig. 9b, the EPR outcomes for 1998–2005 indicate that erosion dominated the Rabigh coastline, being displayed by around 82.81% of all transects, of which 18.55% exhibited erosion of statistical significance, even though the uncertainty was high (± 5.37 myr^{-1}). On the other hand, accretion was exhibited by 17.19% of all transects, by which 1.47% had an accumulation of statistical significance. The highest erosion value –45.89 ± 5.37 myr^{-1} (Table 5; Fig. 9b) was documented in Sharm Rabigh (Fig. 10), while the average erosion rate was –3.83 ± 5.37 myr^{-1}. The southern industrial zone of Khawr al Qadimah had the second-highest rate of erosion of about –30 myr^{-1} ± 5.37 myr^{-1} (Fig. 10). The maximum accretion value of 39.35 ± 5.37 myr^{1} (Table 5; Fig. 9b) was also recorded in Sharm Rabigh (industrial area; Fig. 10), with the average accretion rate of 2.67 myr^{-1}.

4.2.3. Shoreline Changes 2005–2019

Figure 9c shows the average EPR results associated with this final period, for the first time exhibiting the accretional nature of the Rabigh coastline, which has an average annual accretion rate of 1.53 ± 1.41 m. Accretion was displayed by 52.08% of the transects, while erosion of statistical significance was exhibited by just 8.41%. The highest level of accretion was recorded in the northern section of King Abdullah Port (40.90 ± 1.41 myr^{-1}; Table 5; Fig. 9c and 10), while the overall accretion average was 4.74 ± 1.41 myr^{-1}. The second significant area was also located in the southern part of the area at King Abdullah Port (Fig. 10), which had an accretion rate of approximately 31 ± 1.41 myr^{-1}. The maximum erosion rate of –47.21 ± 1.41 myr^{-1} (Table 5; Fig. 9c) was recorded at King Abdullah Port (Figure 10) and was caused by digging and the creation of the port infrastructure, while the average erosion rate was –1.96 myr^{-1}. The erosion of approximately 46 ± 1.41 myr^{-1} (Fig. 9c) observed in the southern part of KAEC (Fig. 10), specifically at Ra's Khurmah, was caused by the construction of water channels.

5. Discussion

It is possible to distinguish patterns of coastal behaviour even though historical data are scarce (Cooper *et al*., 2007). One strategy for outlining the trends of historical coastline development when current hydrodynamic and sediment transport data are unavailable is to use satellite images that are sufficiently precise. In this way, aspects of geomorphology that have a potential impact on coastal management policies can be uncovered. There is a close correlation between coastal city expansion and the existence of public infrastructure facilities. As shown in Table 4 and Fig. 7c, the analysis of long-term spatiotemporal alterations in the form of the coastline over the years of 1986, 1998, 2005, and 2019 in the case of LRR and 1986 and 2019 in the case of EPR revealed temporal erosion trends with an average of –0.5 myr^{-1} and –0.3 myr^{-1} , respectively. Further, human activity was identified as the primary determinant of shoreline kinematics.

LRR was employed to determine spatiotemporal form modifications over the short term for 1986–1998, 1998–2005, and 2005–2019. According to the outcomes of statistical analysis, the entire research period of 33 years was associated with modifications and intervals of erosion and accretion. It is noteworthy that a rise in the seaward aggregation of 14.68 myr^{-1} occurred in the

context of construction related to industrial expansion in 1986–1998 (Fig. 8a and Fig. 9a). Meanwhile, some areas exhibited accumulation factors due to wadi flow, such as Wadi Sa'bar in the south and Wadi al Khalidiyah and Wadi al Halq (Fig. 10) in the middle of the study area. The industrial area in the middle part of the study area was affected by factors causing erosion and determined to have been infrastructure development.

During the period of 1998–2005, the rate of erosion was greater than the rate of accretion. Figures 8b and 9b show erosion fluctuation in the study area, particularly in the Khawr al Qadimah (beginning with the establishment of KAEC in 2005) at the southern part and the industrial area at the middle part (approximately –30 myr^{-1} ± 5.37 myr^{-1} and –14 myr^{-1} ± 5.37 myr^{-1}, respectively). These fluctuations were due to dynamic changes in erosion and accretion phases (Prasetya, 2007). Meanwhile, accretion and erosion rates of 39.35 ± 5.37 myr^{-1} and –45. 89 ± 5.37 myr^{-1}, respectively, were observed in the northern part of the study area (Fig. 10). These were caused by construction and development that included the inner harbour in Sharm Rabigh and the industrial area.

The latest period, 2005–2019, revealed that the most important changes resulting in erosion were associated with anthropogenic activities, such as digging and dredging to enlarge King Abdullah Port (–47.21 ± 1.41 myr^{-1}) and digging of access channels in the southern part of KAEC (–46 ± 1.41 myr^{-1}; Figure 10). At the same time, the significant impact of construction and land reclamation associated with the development of King Abdullah Port led to an erosion rate of 40.90 ± 1.41 myr^{-1} (Fig. 9c). The cumulative increases occurring in this area of the coast up to the end of the research period were significantly shaped by ongoing development (Table 5, Fig. 8c, and d). At the start of port development, erosion was gradually substituted by accretion, as indicated by the EPR modifications, while subsequent infrastructure creation led to fluctuating gains (Fig. 9c). By contrast, stability was more or less maintained in the other shoreline areas throughout the entire research period. Nevertheless, coastal areas displayed accretion, but that was likely due to the beach stabilisation engendered by leisure activities in a few areas, such as KAEC beach. It may also have been related to the seasonal flow of wadis, such as Wadi Sa'bar (Fig. 9c and 10), the Wadi al Halq in the southern part, and Wadi al Khalidiyah in the middle section (Fig. 9c and 10). Also, the erosion indicated that only surficial sediments were lost along the entire frontage.

Despite significant alterations in shoreline behaviour that can be triggered by storms (Cooper and Jackson, 2003), under circumstances of sea level stability and non-fluctuating wave and tidal regimes certain systems may be capable of adapting themselves without the influence of extrinsic forces (Cooper *et al*., 2007). Regarding the area investigated in this work, the overall data indicate an approximately 1.2 m wave height with a duration of 6.7 s, a 0.80 m root-mean-square (RMS) wave height, a 0.70 m mean height, and a 128 m average wavelength. Further, the largest storm waves generally have a south or west direction, despite the fact that the wind usually blows from the north and northwest (Elbisy and Mlybari, 2015). Nevertheless, the fringing reef in the shadow zone protects the Rabigh area from waves (Fig. 10).

An expanding anthropized range beginning in the area of King Abdullah Port and continuing along the KAEC coastline was revealed by comprehensive analysis of the rates over the course of time (Fig. 11a and b). The occurrence of sequential seaward and landward extensions of the Rabigh shoreline in every investigated period was also uncovered by the

analysis. The highest annual rate (erosion or progradation) may be up to 45 m, although this could represent a jetty, dock, artificial promontory, or channel.

5.1 The Implications of Shoreline Modifications for the Rabigh Coastal Area

The coastal environment, including its ecosystems, marine habitats, and benthic communities, have suffered the impact of coastline modifications. Urban industrial activities can have also negative implications in terms of the pollution generated. The coastline has also suffered morphological alterations. The coastal area has been expanded, while a number of reefs have vanished owing to activities of King Abdullah Port or the establishment of KAEC (Fig. 11). It is well known that shoreline morphology is influenced by urban development in coastal areas due to the dredging, excavation, and backfill of coastal sands (Luijendijk *et al*., 2018). Beach erosion has occurred in certain parts of the studied area despite the predominance of accretion, leading to further morphological coastline alterations.

The probability of flood occurrence can be heightened by low-lying area expansion along the coastal fringe. Some parts of Rabigh have been developed in areas where lagoons (Sharm Rabigh and Khawr al Qadimah) or sabkhas (the sabkha around Sharm Rabigh and Khawr al Qadimah and Sabkhat adh Dhinayb; Fig. 10) had once existed. Thus, coastal area alterations can increase the probability of flood occurrence. As shown in Fig. 10, a significant expanse of the area has been constructed on a site that was formerly crossed by wadis (wadi Rabigh in northern part, wadi al Halq and al Khalidiyah in middle part, and wadi Sa'bar in southern part). Thus, research on flood countermeasures and urban storm water infrastructure should consider the likelihood of flash flood occurrence in the area.

The entire coast can be impacted by topographical modifications to the coastline, resulting in subsidence, sabkha formation, and elevation of the saltwater table. The backfilling or dredging of a sizable portion of coastline caused changes to the bathymetry of the coastal area and the coastal geomorphology. The above considerations warrant the formulation of a comprehensive management plan for the coastal resources of the city of Rabigh applicable to future industrial development.

6. Conclusion

The present work employed GIS methods to determine the location of the Rabigh shoreline during the period of 1986–2019 from variously sourced remote sensing data of a diachronic nature. The DSAS generated the statistics regarding the rate of modifications. More specifically, the EPR and LRR tools were used to determine the rate of modifications among sequential periods (1986–1998, 1998–2005, and 2005–2019) and over the whole period, respectively. The extensive period of 33 years investigated spanned the period of economic flourishing promoted by industrial development around Sharm Rabigh and the southern part of the area. This is reflected in the founding of a cement factory, petroleum refinery, and power plant, as well as by the creation of a desalination plant, urban development, and the economic revival in in the northern part of the Rabigh area beginning in 2005. This was most closely associated with the creation of KAEC and King Abdullah Port.

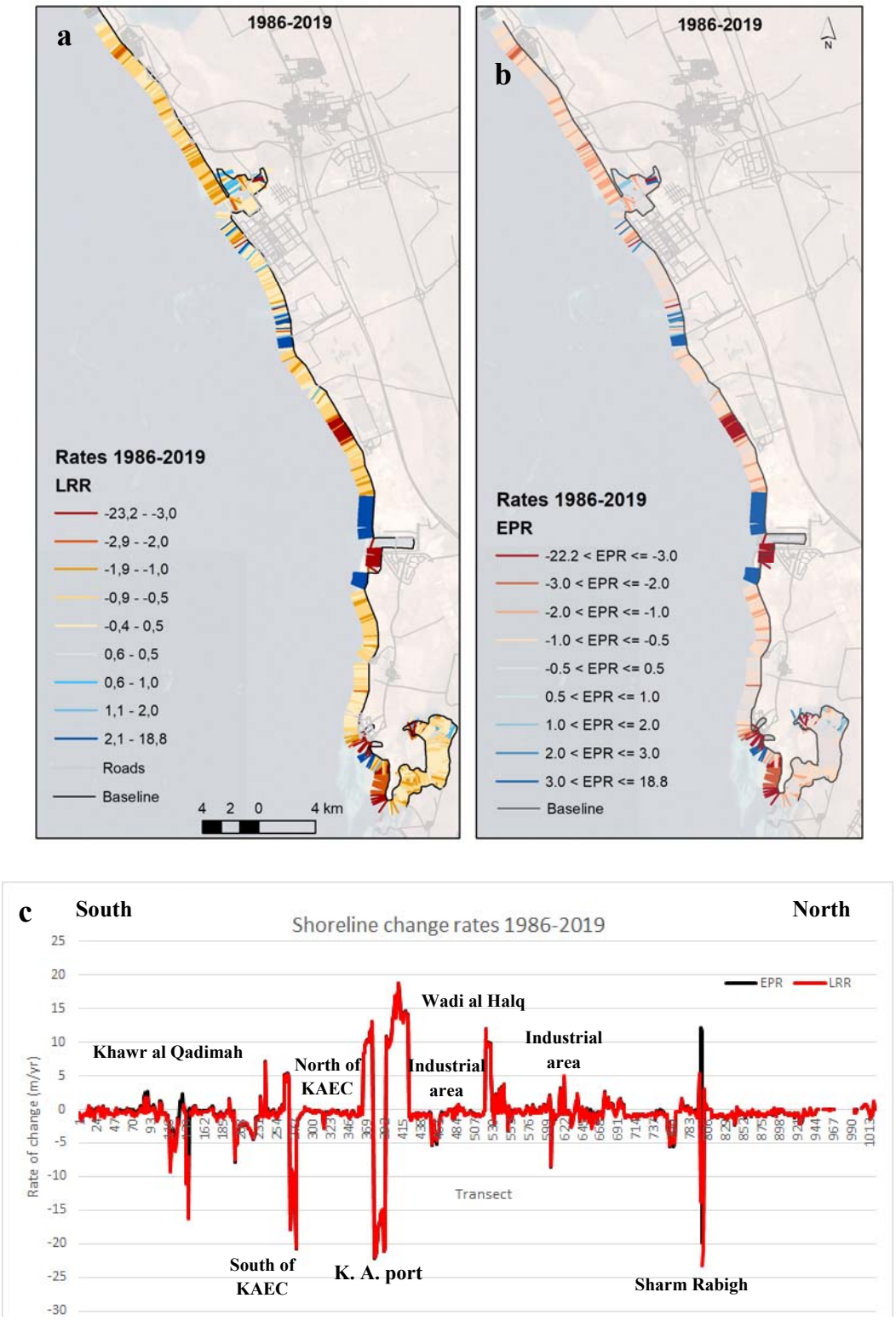

Fig. 7. Long-term shoreline change rates for (a, b) EPR (1986 and 2019) and (c) LRR (1986–2019).

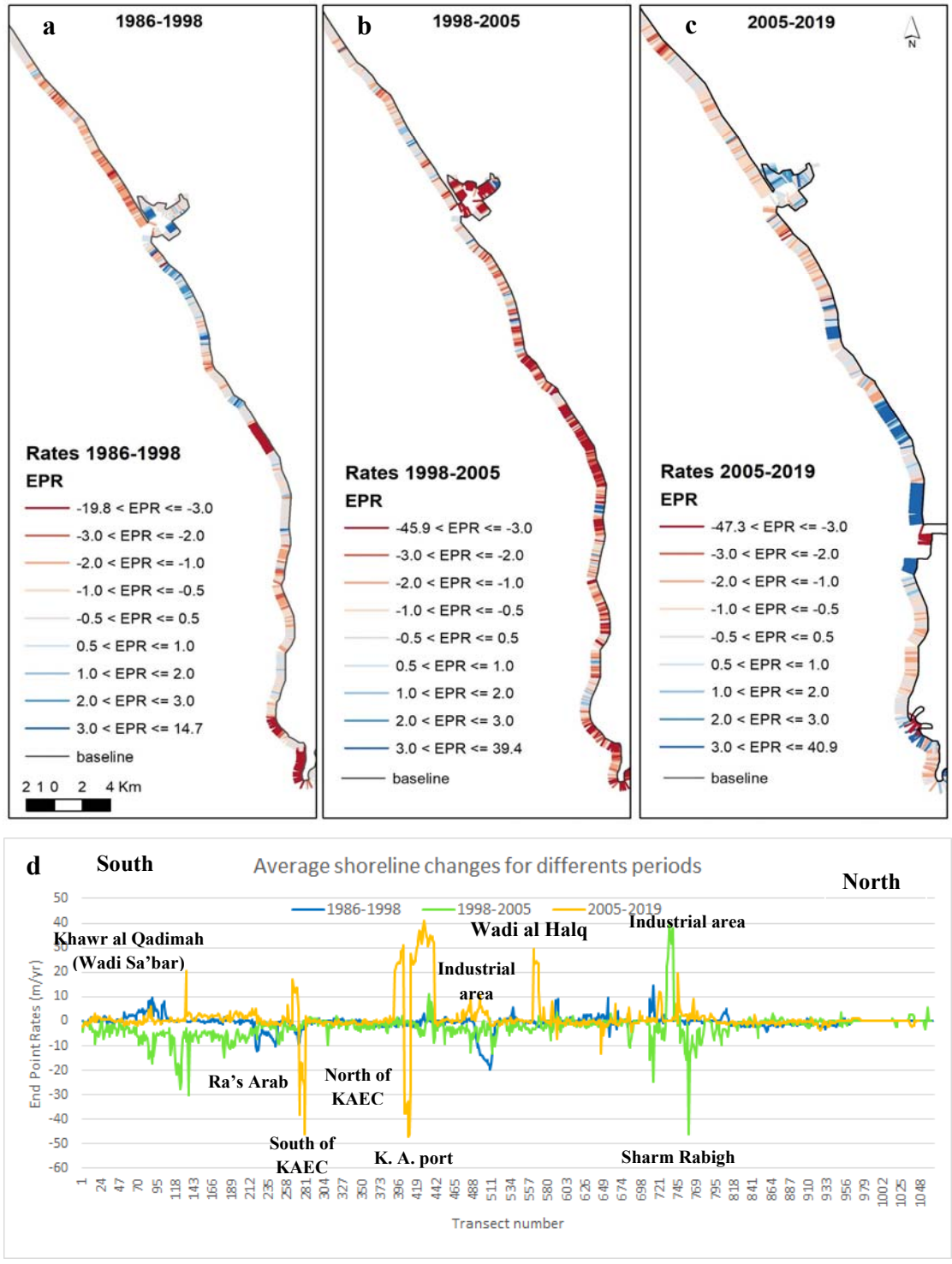

Fig. 8. EPR expressed in myr^{-1} for every transect for the intervals 1986–1998 (a), 199–2005 (b), and 2005–2019 (c). The erosion and accretion rates are represented by the transects with negative and positive values coloured red and blue, respectively; these rates are within the data uncertainty at a level of 95% confidence. (d) Illustration in graphical format and comparative analysis of average rates of modifications for each period.

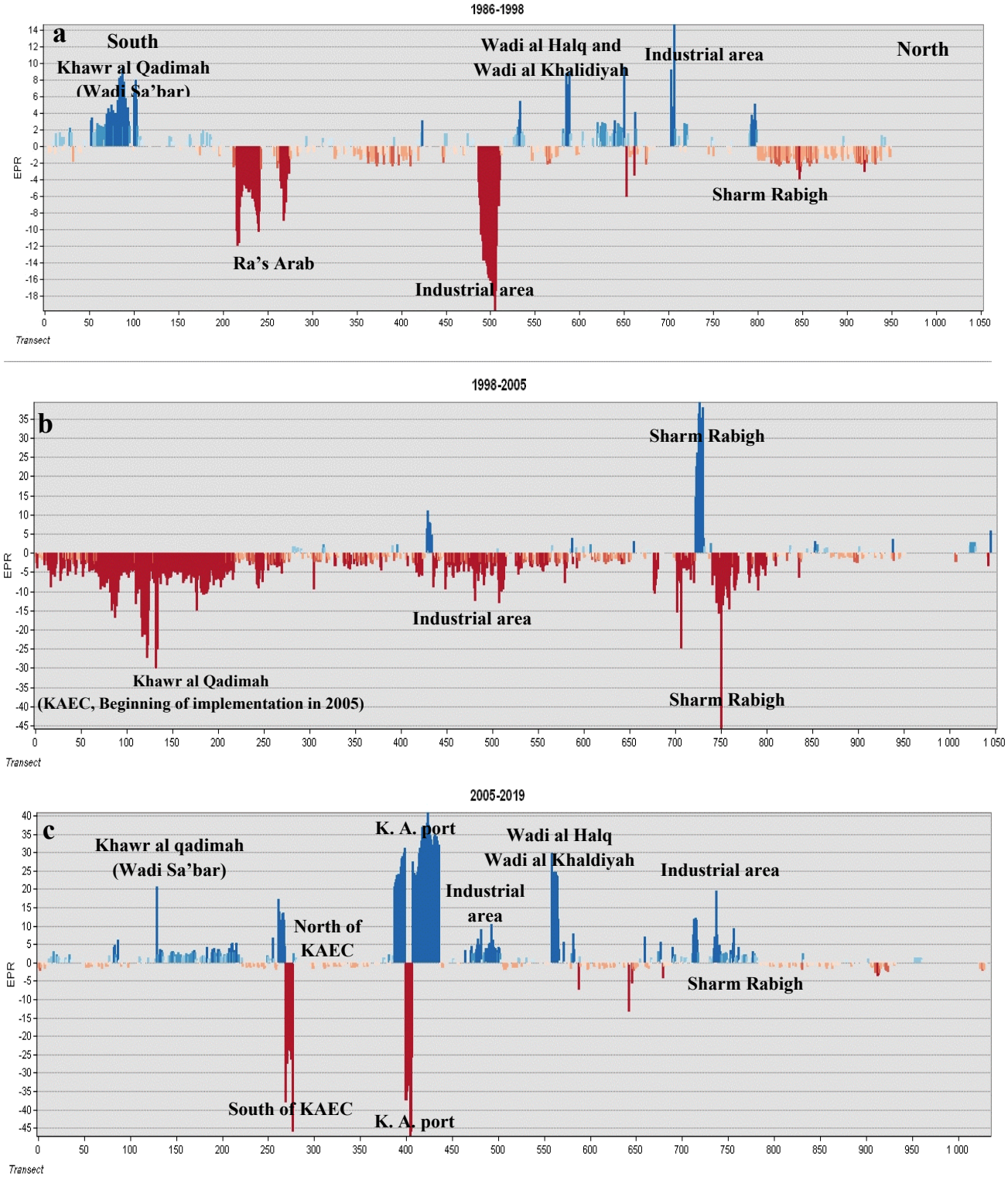

Fig. 9. Transect EPR for 1986–1998 (a), 1998–2005 (b), and 2005-2019 (c). The transects respectively denote erosion and accretion with negative and positive values.

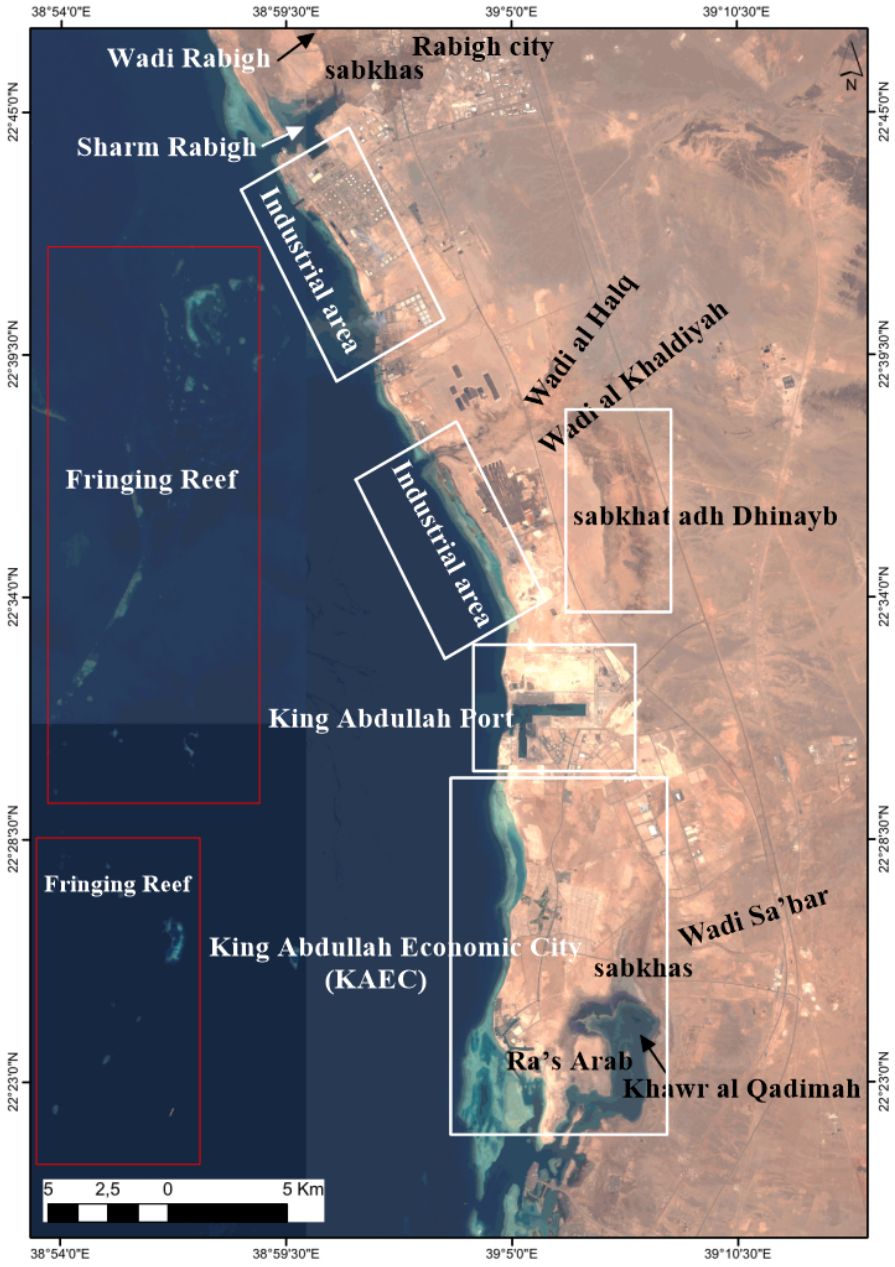

Fig. 10. Coastal locations of the study area.

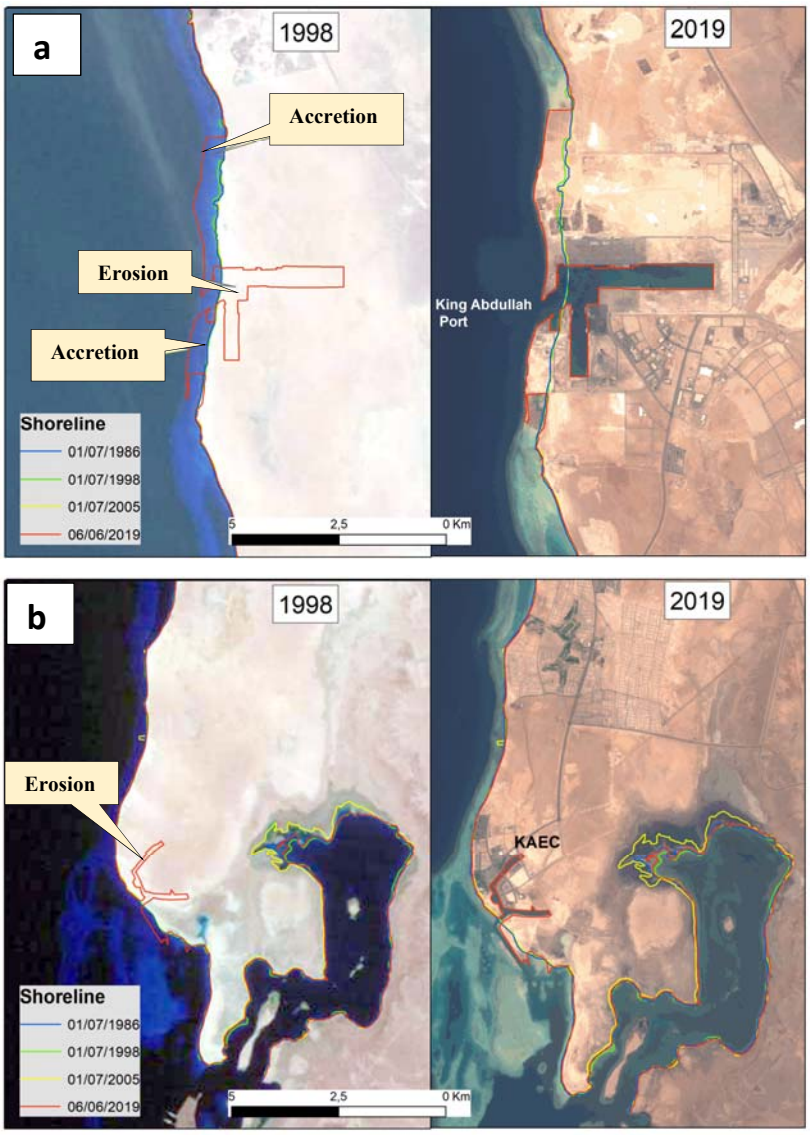

Fig. 11. Illustration of major coastline change areas between 1998 and 2019 around (a) King Abdullah Port and (b) KAEC.

The long-term analysis yielded statistics indicating high levels of fluctuation in the patterns of shoreline erosion and accretion, particularly in Sharm Rabigh, KAEC, and King Abdullah Port, with a few regions experiencing wadi flows. This can be attributed to the development of the central part of the research area, particularly the northern part of KAEC and at King Abdullah Port, as well as the backfilling of sizable portions of the sea, which caused some islands and reefs to vanish. Moreover, dredging and access channel digging in the area of King Abdullah Port, the southern part of KAEC, and Sharm Rabigh have contributed to erosion.

The LRR results revealed that 82.61% of transects exhibited erosion, with the highest annual erosion being –23.22 ± 0.48 m, while the highest annual accretion experienced by the transects was 18.78 ± 0.48 m in the area of King Abdullah Port. The EPR results for the period

of 2005–2019 indicated that the maximum annual erosion rate was greater than 47.21 ± 1.41 m, especially along the littoral in Sharm Rabigh, King Abdullah Port, KAEC, and Ra's Arab area. Regarding accretion rates in the same period, the EPR pointed to the intensification of accretion associated with beach stabilisation caused by economic activities, leisure, and/or tourist facilities in a number of areas. The differences between rates in the short- and long-term indicate alterations in trends and gradual reference line movements between the various periods. Human activity, infrastructure expansion, and the creation of industrial zones, like the Sharm Rabigh, KAEC beach, and the King Abdullah Port, are the prominent determinants of most alterations along the Rabigh coastline. The coastline may become even more vulnerable in the future, such as activities and developments that impact the marine environment and wadi outfalls.

Funding

This research received no external funding.

Conflicts of Interest

The author declares no conflict of interest.

References

Al Sayari, S.S. and **Zotl, J.G.** (1978) *Quaternary period in Saudi Arabia*; Springerverlag, Wien: New York, NY, USA.

Al-Baroudi, M.S. (1990) *The Geomorphology of the Sharms on the east coast of the Red Sea (Arabic)*; Kuwait Geographic Society.

Alharbi, O.A., Phillips, M.R., Williams, A.T., Thomas, T., Hakami, M., Kerbe, J., Niang, A.J., Hermas, E. and **Al-Ghamdi, K.** (2017) Temporal shoreline change and infrastructure influences along the southern Red Sea coast of Saudi Arabia. *Arab J. Geosci*, **10** : 360.

Al-Washmi, H.A. (1999) Sedimentological aspects and environmental conditions recognized from the bottom sediments of Al-Kharrar Lagoon, eastern Red Sea coastal plain, Saudi Arabia. *J. KAU Mar. Sci*, **10** : 71–87.

Bagli, S. and **Soille, P.** (2003) Morhological automatic extraction of pan-European coastline from Landsat ETM+images. In International symposium on GIS and computer cartography for coastal zone management, Genova, October, pp : 256–269.

Balica, S.F., Wright, N.G. and **Van der Meulen, F.** (2012) A flood vulnerability index for coastal cities and its use in assessing climate change impacts. *Nat Hazards*, **64** : 73–105.

Basaham, A.S. (2008) Mineralogical and chemical composition of the mud fraction from the surface sediments of Sharm Al-Kharrar, a Red Sea coastal lagoon. *Oceanologia*, **50** : 557–575.

Basiouny, M.E., El Kafrawy, S.B., Ghanem, E.A. and **Taha, A.S.** (2017) Shoreline change rate detection and future prediction using remote sensing and GIS techniques: a case study of Ras EL-Hekma, north western coast, Egypt. *J Geogr Environ. Earth Sci. Int*., **9** : 1–14

Behairy, A.K.A., Rao, D.N.V.N. and **El-Shater, A.** (1991) A siliciclastic coastal sabkha, Red Sea coast, Saudi Arabia. *Journal of the Faculty of Marine Science*, **2** : 65–77.

Benedet, L., Klein, A.H.F. and **Hsu, J.R.C.** (2004) Practical insights and applicability of empirical bay shape equations, In *Proceedings of the 29th International Conference Coastal Engineering, Lisbon, Portugal, 19–24 September; Jane McKee Smith.*

Carter, R.W.G. (1988) *Coastal Environments, An Introduction to the Physical, Ecological and Cultural Systems of Coastlines*; Academic Press, London, UK.

Chenthamil Selvan, S., Kankara, R.S. and **Rajan, B.** (2014) Assessment of shoreline changes along Karnataka coast, India using GIS & Remote sensing techniques. *Indian J. Mar. Sci*., **43** : 1286-1291.

Cooper, J.A.G. and **Jackson, D.W.T.** (2003) Geomorphological and dynamic constraints on mesoscale coastal response to storms, Western Ireland. In Coastal Sediments '07: Proceedings 6th International Symposium on Coastal Engineering and Science of Coastal Sediment Processes; American Society of Civil Engineers: Reston, VA, USA; pp. 3015–3024.

Cooper, J.A.G., McKenna, J., Jackson, D.W.T. and **O'Connor, M.** (2007) Meso-scale coastal behaviour related to morphological self-adjustment. *Geological Society of America*, **35** : 187–190.

Crowell, M. and **Leatherman, S.P.** (1999) Coastal erosion mapping and management. *J. Coast. Res.*, **SI28**, 196 p.

Crowell, M., Leatherman, S.P. and **Buckley, M.K.** (1991) Historical Shoreline Change: Error Analysis and Mapping Accuracy. *J. Coast. Res.*, **7** : 839–852.

Dewidar, K. (2011) Changes in the Shoreline Position Caused by Natural Processes for Coastline of Marsa Alam–Hamata, Red Sea, Egypt. *Inter. J. of Geosc*., **2**, 523.

Dobroniak, C. and **Anthony, E.J.** (2002) Short-term morphological expression of dune sand recycling on a microtidal, wave-exposed estuarine shoreline. *J. Coast. Res.*, **SI35** : 240–248.

Douglas, B.C. and **Crowell, M.** (2000) Long-term shoreline position predictions and error propagation. *J. Coast. Res.*, **16** : 145–152

Durgaprasada Rao. N.V.N. and **Behairy, A.K.A.** (1986) Nature and composition of shorezone sediments between Jeddah and Yanbu, Eastern Red Sea, Saudi Arabia. *Marine Geology*, **70** : 412–441.

El-Asmar, H.M. (2002) Short term coastal changes along Damiette – port said coast northwest of the Nile Delta, Egypt. *J. Coast. Res.*, **18** : 433–441.

El-Asmar, H.M.,Ahmed, M.H., El-Kafrawy, S.B., Oubid-Allah, A.H., Mohamed, T.A. and **Khaled, M.A.** (2015) Monitoring and Assessing the Coastal Ecosystem at Hurghada, Red Sea Coast, Egypt. *J. of Envir. and Ear. Scie.*, **5** : 144–160.

Elbisy, M.S. and **Mlybari, E.A.** (2015) Comprehensive environmental management of the construction of the marine works of the Rabigh coastal power plant project on the Red Sea, Saudi Arabia. *Inter. J. Envir. Plan. and Manag.*, **1** : 144–156.

El-Raey, M., Sharaf El-Din, S.H., Khafagy, A.A. and **AboZed, A.I.** (1999) Remote sensing of beach erosion/accretion patterns along Damietta–port said shoreline, Egypt. *Int. J. Remote Sens.*, **20** : 1087–1106.

Esteves L.S., Toldo E.E. Jr. and **Dillenburg, S.R.** (2002) Long and short- term coastal erosion in southern Brazil. *J. Coast. Res.*, **SI35** : 273–282.

Esteves, L.S., Williams, J.J. and **Dillenbrug, S.R.** (2006) Seasonal and interannual influences on the patterns of shoreline changes in Rio Grande do Sul, southern Brazil. *J. Coast. Res.*, **22**, 1076–1093.

Granja, H.M. and **Carvalho, G.S.** (2000) Inland Beach migration (beach erosion) and the coastal zone management (experience of the northwest coastal zone of Portugal). *Period Biol*., **102** : 413–424.

Hapke, C.J., Himmelstoss, E.A., Kratzmann, M.G., List, J.H. and **Thieler, E.R.** (2011) *National assessment of shoreline change: Historical shoreline change along the New England and Mid-Atlantic coasts*; Open-File Report 2010-1118; U.S. Geological Survey.

Himmelstoss, E.A., Henderson, R.E., Kratzmann, M. G. and **Farris, A.S.** (2018) *Digital Shoreline Analysis System (DSAS) version 5.0 user guide (No. 2018-1179)*; Open-File Report 2018–1179; U.S. Geological Survey, https://doi.org/10.3133/ofr20181179.

Komar, P.D. (1998) *Beach processes and sedimentation*, 2nd ed.; Prentice Hall: New Jersey, USA.

Leatherman, S.P. (2003) Shoreline change mapping and management along the U.S. East Coast. *J. Coast. Res.*, **SI38** : 5–13.

Liu, H. and **Jezek, K.C.** (2004) Automated extraction of coastline from satellite imagery by integrating canny edge detection and locally adaptive thresholding methods. *Int. J. Remote Sens.*, **25** : 937–958.

Luijendijk, A., Hagenaars, G., Ranasinghe, R., Baart, F., Donchyts, G. and **Aarninkhof, S.** (2018) The state of the world's beaches. *Scientific reports*, **8** : 1–11.

Madah, F., Mayerle, R., Bruss, G. and **Bento, J.** (2015) Characteristics of Tides in the Red Sea Region, a Numerical Model Study. *Open J. Mar. Sci.*, **5** : 193.

Maune, D.F. (2007) Digital Elevation Model Technologies and Applications: The DEM User's Manual, second Edition. American Society for Photogrammetry and remote Sensing. Bethesda, Maryland.

Mills, J.P., Buckley S.J., Mitchell H.L., Clarke P.J. and **Edwards S.J.** (2005) A geomatics data integration technique for coastal change monitoring. *Earth Surf. Process*, **30** : 651–664.

Moore, L.J. (2000) Shoreline mapping techniques. *J. Coast. Res.*, **16** : 111–124.

Morcos, S.A. (1970) Physical and chemical oceanography of the Red Sea. *Oceanogr. Mar. Biol.*, **8** : 73–202.

Natesan, U., Parthasarathy, A., Vishnunath, R., Kumar, G. E. J. and **Ferrer, V. A.** (2015) Monitoring longterm shoreline changes along Tamil Nadu, India using geospatial techniques. Aquatic Procedia, **4. Icwrcoe**: 325-332.

Newsham, R., Belson, P.S., Tragheim, D.G. and **Denniss, A.M.** (2002) Determination and prediction of sediment yields from recession of the Holderness coast, N.E. England. *J Coast Conserv*., **8** : 49–54.

Niang, A. (2020) Monitoring long-term shoreline changes along Yanbu, Kingdom of Saudi Arabia using remote sensing and GIS techniques. Journal of Taibah University for Science, **14**.1: 762-776.

Nofal, R. and **Abboud, I.A.** (2016) Geomorphological evolution of marine heads on the eastern coast of Red Sea at Saudi Arabian region, using remote sensing techniques. *Arab. J. Geosci*., **9** : 1–15.

O'Connor, M.O., Cooper, J.A.G. and **Jackson, D.W.T.** (2007) Morphological Behaviour of Headland-Embayment and Inlet-Associated Beaches, Northwest Ireland. *J. Coast. Res.*, **SI59** : 626–630.

Pajak, M.J. and **Leatherman, S.** (2002) The high water line as shoreline indicator. *J. Coast. Res.*, **18** (2) : 329–337

Parker, B.B. (2003) The Difficulties in Measuring a Consistently Defined Shoreline – The Problem of Vertical Referencing. *J. Coast. Res.*, **SI38** : 44–56.

Patzert, W.C. (1974) Wind-induced reversal in Red Sea circulation. *Deep-Sea Research*, **21** : 109–121.

Pethick, J. (1996) The sustainable use of coasts: monitoring, modelling and management. *Stud Eur Coastal Manag*., 83–92.

Pranzini, E. and **Williams, A.T.** (2013) *Coastal erosion and protection in Europe*; Routledge/Earthscan, London, UK, pp 54.

Prasetya, G. (2007) The role of coastal forests and trees in protecting against coastal erosion. In *Regional Technical Workshop. Coastal protection in the aftermath of the Indian Ocean tsunamis: what role for forests and trees?*, Khao Lak, Thailand, 28-31 August 2006; Braatz, S., Fortuna, S., Broadhead, J. and Leslie, R., 103–132.

Rogers, J., Hamer, B., Brampton, A., Challinor, S., Glennerster, M., Brenton, P. and **Bradbury, A.** (2010) *Beach management manual*, 2nd ed.; CIRIA: London, UK.

Sagheer, A.A., Humade, A. and **Al-Jabali, A.M.** (2011) Monitoring of coastline changes along the Red Sea, Yemen based on remote sensing technique. *Global Geology*, **14** : 241–248.

Selvavinayagam, K. (2008) *Shoreline change monitoring in Tuticorine coast using remote sensing and GIS tools*; News and Society: Environmental.

Short, A.D. and **Masselink, G.** (1999) Embayed and structurally controlled beaches. In *Handbook of beach and Shoreface Morphodynamics*; Short, A.D., Ed.; Wiley: Chichester, UK, pp : 230–249.

Silva, J.F. and **Duck, R.W.** (2006) Changing use and hydromorphological adjustment in a coastal lagoon-estuarine system, the ria de Aveiro, Portugal. *Sediment Dynamics and the Hydromorphology of Fluvial Systems*, **306** : 197–204.

Tett, P., Gilpin, L., Svendsen, H., Erlandsson, C.P., Larsson, U., Kratzer, S., Fouilland, E., Janzen, C., Lee, J., Grenz, C., Newton, A., Ferreira, J.G. and **Fernades, T., Scory, S.** (2003) Eutrophication and some European waters of restricted exchange. *Cont. Shelf Res.*, **23** : 1635–1671.

Thieler, E.R., Himmelstoss, E.A., Zichichi, J.L. and **Ergul, A.** (2017) *Digital Shoreline Analysis System (DSAS) version 4.0—An ArcGIS extension for calculating shoreline change (ver. 4.4, July 2017)*; Open-File Report 2008-1278; U.S. Geological Survey.

Thomas, T., Phillips M.R. and **Williams, A.T.** (2010) Mesoscale evolution of a headland bay: beach rotation process. *Geomorphology*, **123** : 129– 141.

Thomas, T., Phillips, M.R., Williams, A.T. and **Jenkins, R.E.** (2011) A multicentury record of linked nearshore and coastal change. *Earth Surf. Process*, **36** : 995–1006.

Thomas, T., Phillips, M.R., Williams, A.T. and **Jenkins, R.E.** (2011) Short-term beach rotation, wave climate and the North Atlantic oscillation (NAO). *Prog Phys Geogr*., **35** : 333–352.

Wernette, P., Shortridge, A., Lusch, D.P. and **Arbogast, A.F.** (2017) Accounting for positional uncertainty in historical shoreline change analysis without ground reference information. *Int. J. Remote Sens.*, **38** (13) : 3906–3922.

Williams, A.T., Pond, K., Ergin, A. and **Cullis, M.J.** (2013) The hazards of beach litter. In *Coastal Hazards*; Springer: Dordrecht, Netherlands, 753–780.

Woodroffe, C.D. (2002) *Coasts, form, processes and evolution*; Cambridge University Press: Cambridge, UK.

Zhang, K., Huang, W., Douglas, B.C., Leatherman, S. (2002) Shoreline position variability and long-term trend analysis. *Shore Beach*, **70** : 31–35.

Zhang, X., Pan, D., Chen, J., Zhao, J., Zhu, Q. and **Huang, H.** (2014) Evaluation of Coastline Changes under Human Intervention Using Multi-Temporal High-Resolution Images: A Case Study of the Zhoushan Islands, China. *Remote Sens*., **6** : 9930–9950

.

تحليل تغير الخط الساحلي على طول ساحل رابغ بالمملكة العربية السعودية باستخدام صور الأقمار الصناعية متعددة الأزمنة

عمر علي الحربي

قسم الجغرافيا، كلية العلوم الاجتماعية، جامعة أم القرى، مكة المكرمة، المملكة العربية السعودية

oaoharbi@uqu.edu.sa

المستخلص. يوجد نقص في فهم تأثير الأنشطة الساحلية على التغيرات الطارئة على ساحل البحر الأحمر بالمملكة العربية السعودية. يستفيد العمل الحالي من بيانات الأقمار الصناعية متعددة الأزمنة وتطبيق نظام تحليل الخط الساحلي الرقمي (DSAS) للتحقيق في التغيرات في موقع الخط الساحلي على طول منطقة رابغ الساحلية خلال الفترة 1986–2019. ولتقييم الاتجاهات على المدى القصير والطويل، تم استخدام معدل نقطة النهاية (EPR) ومعدل الانحدار الخطي (LRR) لتحديد المعدلات التي حدثت بها تغييرات الخط الساحلي. ووفقًا لتقنية LRR، كان الحد الأقصى للتآكل والحد الأقصى للتراكم −23.22 و18.8 myr^{-1} على التوالي، بينما وفقًا لتقنية EPR، كان الحد الأقصى لمعدلات التآكل والتراكم −47.30 و40.90 myr^{-1} على التوالي. وقد دعم النشاط البشري، بما في ذلك توسيع البنية التحتية، وتطوير الموانئ، وإنشاء مناطق صناعية، أهم التغيرات في هيكل الخط الساحلي. ومن هذا المنظور، يقدم العمل الحالي نظرة عامة على مدى التأثيرات السلبية المحتملة على النظام الساحلي والتداعيات المحتملة.

الكلمات المفتاحية: الاستشعار عن بعد، تغير الخط الساحلي، تآكل السواحل، التراكم، DSAS، الأنشطة البشرية، رابغ، البحر الأحمر، المملكة العربية السعودية.